Geophys. J. Int. (2007) **171,** 847–856 doi: 10.1111/j.1365-246X.2007.03575.x

Finite-frequency sensitivity kernels for head waves

Zhigang Zhang,[1] Yang Shen[1] and Li Zhao[2]

[1] *Graduate School of Oceanography, University of Rhode Island, Narragansett, RI* 02882*, USA. E-mail: zzhang@gso.uri.edu*
[2] *Institute of Earth Sciences, Academia Sinica, Taipei* 115*, Taiwan*

Accepted 2007 August 4. Received 2007 July 10; in original form 2007 January 9

SUMMARY

Head waves are extremely important in determining the structure of the predominantly layered Earth. While several recent studies have shown the diffractive nature and the 3-D Fréchet kernels of finite-frequency turning waves, analogues of head waves in a continuous velocity structure, the finite-frequency effects and sensitivity kernels of head waves are yet to be carefully examined. We present the results of a numerical study focusing on the finite-frequency effects of head waves. Our model has a low-velocity layer over a high-velocity half-space and a cylindrical-shaped velocity perturbation placed beneath the interface at different locations. A 3-D finite-difference method is used to calculate synthetic waveforms. Traveltime and amplitude anomalies are measured by the cross-correlation of synthetic seismograms from models with and without the velocity perturbation and are compared to the 3-D sensitivity kernels constructed from full waveform simulations. The results show that the head wave arrival-time and amplitude are influenced by the velocity structure surrounding the ray path in a pattern that is consistent with the Fresnel zones. Unlike the 'banana–doughnut' traveltime sensitivity kernels of turning waves, the traveltime sensitivity of the head wave along the ray path below the interface is weak, but non-zero. Below the ray path, the traveltime sensitivity reaches the maximum (absolute value) at a depth that depends on the wavelength and propagation distance. The sensitivity kernels vary with the vertical velocity gradient in the lower layer, but the variation is relatively small at short propagation distances when the vertical velocity gradient is within the range of the commonly accepted values. Finally, the depression or shoaling of the interface results in increased or decreased sensitivities, respectively, beneath the interface topography.

Key words: finite-frequency tomography, Fréchet kernels, head waves, Pn, waveform simulation.

INTRODUCTION

Head waves are known as refracted waves that propagate along and immediately next to the layer interfaces in the higher velocity layers (Berry & West 1966; Cerveny & Ravindra 1971; Lay & Wallace 1995; Aki & Richards 2002). They have been used to map interface velocity structure at various scales and in different regions (e.g. Bannister *et al*. 1991; Nolet *et al*. 1998; Brazier *et al*. 2000; Ritzwoller *et al*. 2002). In the studies of the crust and uppermost mantle, Pn and Sn are often attributed to be the compressional and shear head waves propagating in the uppermost mantle, though strictly a pure head wave is defined in models of uniform plane layers. In models of spherical layers and/or models having a positive velocity gradient beneath the Moho, Pn or Sn evolves into a mantle turning wave plus interference waves or whispering gallery waves at large epicentral distances (e.g. Menke & Richards 1980; Nowack & Stacy 2002). Within a few hundred kilometers, Pn and Sn waves propagate near the top of the mantle like head waves. However, at epicentral distances of 10° or more, Pn and Sn ray paths may be bottoming within the lower lithospheric lid with large regional variation in their characteristics. Pn waves along many profiles in eastern North America, for example, consist principally of turning waves, while those in the Western United States appear more like head waves (Langston 1982). Because of the complex nature and regional variation, Pn is often simply defined in a heuristic approach as the *P* wave arriving between epicentral distances of approximately 2° and 15° with a phase velocity between 7.8 and 8.3 km s^{-1}. The distinction between the ordinary head wave and deeper-turning phases is usually not made.

Because the Pn phase is the first arrival at regional epicentral distances (∼2°–15°), it has been widely used in detecting and locating seismic events as well as inferring the velocity and attenuation structure of the uppermost mantle. In conventional Pn or Sn traveltime tomography, traveltime variations in Pn or Sn waves are usually attributed to velocity changes right beneath the Moho and in the crust near the source and receiver under ray approximation. Consequently conventional Pn and Sn tomographic inversions solve only the 2-D problems of lateral variations in the uppermost mantle and provide

© 2007 The Authors
Journal compilation © 2007 RAS

no constraints on the vertical structure beneath the Moho. The simplification of horizontal Pn and Sn propagation introduces a bias in the predicted traveltimes since real waves dive beneath the Moho to depths that depend on the vertical velocity gradient and epicentral distance. To correct for this deficiency in theory in Pn tomography, Zhao & Xie (1993) and Ritzwoller *et al.* (2002) used a regionalized correction as a function of epicentral distance. However, in places with anomalous vertical velocity gradients, this regionalized correction may be inadequate. In a study of the mantle velocity structure beneath China, Hearn *et al.* (2004) tried to accommodate the first-order effect of the vertical velocity gradient in the mantle lid by splitting the Pn data set into two groups having epicentral distances smaller or greater than 9.5°. Separate images, which roughly represent the velocity structures of the upper- and lower-lithospheric lid, respectively, were obtained using the two groups of data sets.

It has been recognized for many years that scattering in the upper-mantle plays a significant role in Pn-wave propagation, and may be responsible for producing the Pn coda (Båth 1966; Menke & Richards 1983; Morozov *et al.* 1998; Ryberg *et al*. 2000; Tittgemeyer *et al*. 2000). There is therefore, a large gap between the assumptions in Pn and Sn tomographic studies to date and the propagation of real Pn and Sn waves. Since tomographic inversions are only as good as the forward problem that describes wave propagation, a practical theory providing a more accurate representation of realistic head waves is needed. The recent development of the finite-frequency seismic theory has made it possible to extract more information from broad-band seismograms. While previous studies have shown the diffractive nature and the 3-D Fréchet kernels of finite-frequency turning waves (Dahlen *et al*. 2000; Hung *et al*. 2000; Zhao *et al*. 2000; Tromp *et al*. 2005; Zhao *et al*. 2005; Liu & Tromp 2006; Zhao & Jordan 2006), analogues of head waves in a continuous velocity structure, the finite-frequency effects and sensitivity kernels of head waves, which have features distinctly different from turning waves (Aki & Richards 2002), are yet to be carefully examined.

In this paper, we document the finite-frequency behaviours of head waves as exemplified by Pn in numerical models with uniform layers as well as Pn in models with a vertical velocity gradient and relatively short propagation distances. We expect the finite-frequency behaviours of Sn waves should be similar to those of Pn waves. We used a 3-D, fourth-order, staggered-grid finite-difference method (Olsen 1994) to simulate head wave propagation. Our model has a low-velocity layer over a high-velocity half-space, and a cylindrical-shaped velocity anomaly placed below the interface at different locations. Finite-frequency traveltime and amplitude anomalies are measured by the cross-correlation of synthetic seismograms from models with and without the velocity anomaly and compared with the 3-D sensitivity kernels constructed from full waveform simulations. Our results show that the finite-frequency sensitivity kernels for head waves are significantly different from those of turning waves as well as the predictions of ray theory. The head wave arrival-time and amplitude are influenced by the 3-D velocity structure surrounding the ray path in a pattern that is generally consistent with the Fresnel zones.

WAVEFORM SIMULATION AND CROSS-CORRELATION

We carried out a waveform simulation study to understand the behaviours of finite frequency head waves in a simple and direct way and obtain traveltime and amplitude measurements for a comparison with the 3-D Fréchet kernels presented in the following section. A 3-D, staggered-grid, finite-difference method based on Olsen (1994) and Marcinkovich & Olsen (2003) was used to calculate the synthetic waveforms. We started with a simple model, in which a flat interface separates a low-velocity layer over a high-velocity half-space (Fig. 1). The *P*, *S* velocities and the density of the first layer are 5207 m s^{-1}, 3189 m s^{-1} and 2950 kg m^{-3}, respectively; those of the half-space 9058 m s^{-1}, 5307 m s^{-1} and 3992 kg m^{-3}. Without the loss of generality, the layer velocities and thicknesses represent a gross simplification of the crust and upper-mantle structure and result in a velocity contrast at the interface that is probably larger than that at the Moho in the real Earth. This deviation from the real Earth, however, allows us to use a smaller model with lower computational costs because of a shorter Pg-Pn crossover distance. We put a cylindrical-shaped velocity anomaly having a velocity reduction of 6 per cent, a radius of 3.4 km, and a height of 2.0 km within the high-velocity layer, and measure the phase and amplitude perturbations by cross-correlating the vertical component of the synthetic head wave waveforms for models with and without the velocity anomaly (Fig. 2). This is repeated horizontally every 1.6 km in the radial and transverse directions and at various distances below the layer interface. All results shown in this paper are calculated from the vertical component of the receiver.

Because of the symmetry about the vertical plane containing the source and receiver, we only move the velocity anomaly on one side of the symmetry plane. The finite-difference model has a regular grid of 280 × 301 × 126 in the radial, transverse and vertical directions, with a grid spacing of 400 m. For simplicity, we choose an explosive source with the source time function $M(t)$:

$$M(t) = \int_0^t e^{-\alpha(t-t_0)^2}\,\mathrm{d}t, \tag{1}$$

where α equals to 20, which means the source time function has a dominant period of about 1.2 s. The Q values for *P* and *S* waves in the model are set at arbitrarily high values so we ignore attenuation and focus on the elastic behaviours. We use a time step of 0.02 s that satisfies the stability condition. The maximum wave propagation time is 20 s. Each calculation takes about 55 min on a Linux workstation with a 3.4 GHz Xeon processor and 2 Gb of memory.

Fig. 3 shows the Pn traveltime delays measured from waveform cross-correlation. The results are clearly very different from those predicted by ray theory. While in ray theory traveltime anomaly is sensitive only to velocity perturbation along the ray path and the sensitivity of the ray below the interface is the same along the ray path, our results show that finite-frequency head waves are sensitive to the 3-D structure in a more complex way. The most striking feature of the traveltime delays is the local maxima around the two piercing points on the interface, where the ray path of the head wave enters and leaves the high-velocity layer near the source and receiver, respectively. We note the asymmetry about the source and receiver in the traveltime delays, which can be attributed to the fact that the source is much closer to the interface than the receiver. In this particular example the near-field terms dominate at the interface near the source. This can also be understood from the 3-D Fréchet kernels calculated from full wave simulations in the following section. Interestingly there is a local minimum within the region of higher values around the piercing point on the receiver side (Fig. 4). This feature is not observed on the source side.

For turning waves, one of the most important differences between the finite-frequency traveltime Fréchet kernels and ray theoretical prediction is that the finite-frequency kernels for traveltimes measured by waveform cross-correlation have a hollow (minimum) sensitivity region surrounding the geometrical ray (e.g. Dahlen *et al.*

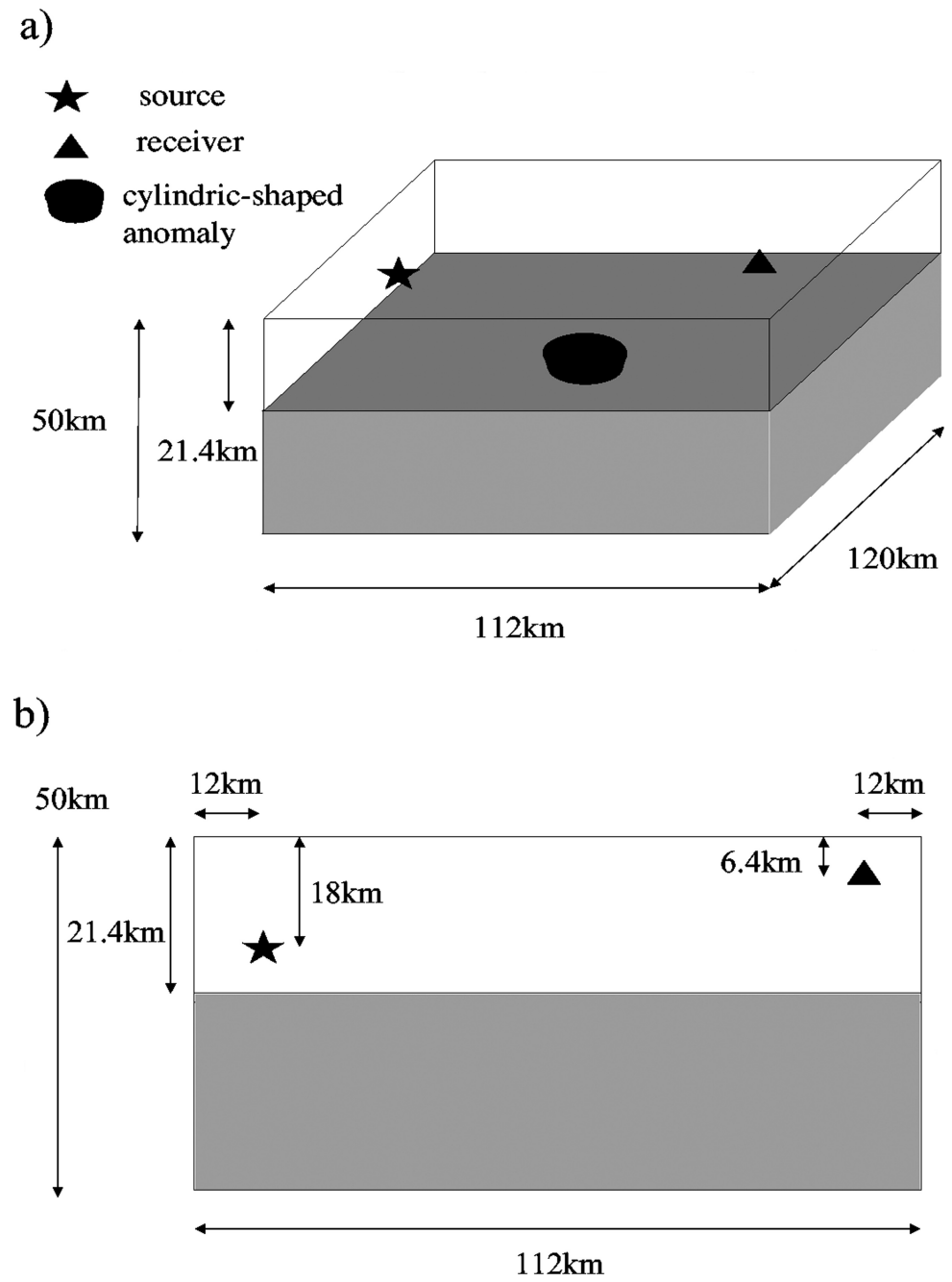


Figure 1. Schematic illustration of the geometry of the two-layer model. The dimensions of the model are marked. (a) Star represents the explosive source used in wave simulations. Triangle marks the receiver. Dark disk represents a cylindrical-shaped velocity perturbation beneath the interface. (b) The vertical profile containing the source and the receiver. The model and the source–receiver geometry are designed so that the head wave is separated clearly from other phases, including waves reflected from the side and bottom boundaries due to imperfect absorption of seismic energy at the boundaries. See text for the velocities and densities of the layers.

2000; Hung *et al.* 2000; Zhao *et al.* 2000). Unlike the 'banana–doughnut' traveltime sensitivity kernels of turning waves, the traveltime anomaly, and thus the traveltime sensitivity, of the head wave, is weak but non-zero along the ray path right beneath the interface (Fig. 3a). In contrast, when the velocity perturbation is a few kilometres directly below the ray path and the interface, the delays approaches zero (Figs 3b and 4a).

The pattern of the positive and negative delays due to the same low-velocity perturbation at different locations matches well with the predicted Fresnel zones, the volumes within which scatterers generate scattered waves whose phases are delayed by a successive half-period of the reference wave. Fig. 5 shows the first, second, and third Fresnel zones delineated by the lines superimposed on the plan view of the traveltime delays for the velocity perturbation right beneath the interface. As expected the traveltime delays are most sensitive to velocity perturbations within the first Fresnel zone, which has a maximum half width of ∼13 km about half way between the source and receiver.

© 2007 The Authors, *GJI*, **171,** 847–856
Journal compilation © 2007 RAS

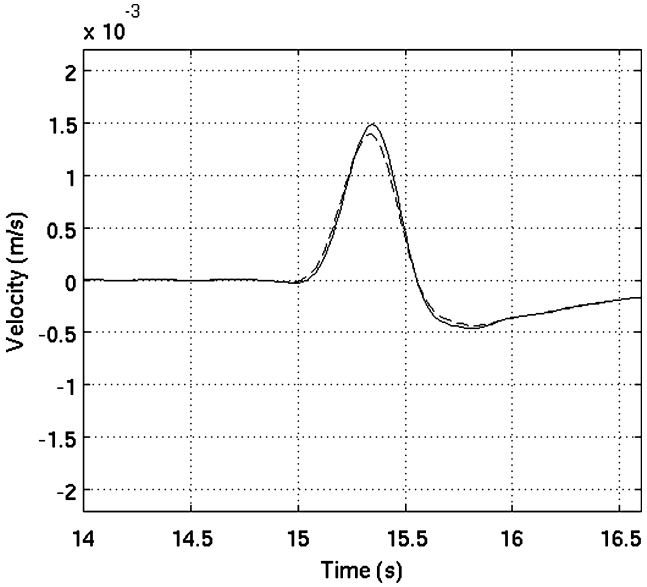


Figure 2. Comparison of the head wave calculated from the reference model (dash line) and the model with a low-velocity anomaly located 9.6 km from the source, between the source and receiver and right beneath the interface (solid line). The horizontal axis is time after the origin of the explosive source. The vertical axis is the velocity of particle motion at the receiver.

SENSITIVITY KERNELS

The simulation and direct waveform cross-correlation yield valuable insights into the behaviours of finite-frequency head waves and provide 'ground truth' measurements to be compared with the predictions from more sophisticated methods. However, this approach is computationally intense and impractical for real observational problems. In order to achieve a fuller understanding of the structural sensitivity of finite-frequency head waves and reduce the computation cost, we obtain the Fréchet kernels of the head waves using the scattering-integral method of Zhao *et al*. (2005), which applies the principle of reciprocity for the Green's tensors between the points in the 3-D model and the receiver. As in Dahlen *et al*. (2000) and Zhao *et al.* (2000), we define the traveltime delay measured by waveform cross-correlation between the reference and perturbed waveforms as

$$\delta\tau_p = -\frac{\int_{t_1}^{t_2} \dot{\tilde{u}}(t)\delta u(t)\mathrm{d}t}{\int_{t_1}^{t_2} |\dot{\tilde{u}}(t)|^2\mathrm{d}t}. \quad (2)$$

We define the amplitude anomaly as

$$\delta A = -\frac{\int_{t_1}^{t_2} \tilde{u}(t)\delta u(t)\mathrm{d}t}{\int_{t_1}^{t_2} |\tilde{u}(t)|^2\mathrm{d}t}. \quad (3)$$

In eqs (2) and (3), $\tilde{u}(t)$ is the synthetic waveform (displacement) for the reference model, $\delta u(t)$ is the waveform perturbation, and $\dot{\tilde{u}}(t)$ is the time derivative of displacement (velocity).

Fig. 6(a) shows the sensitivity kernels for the Pn wave on the vertical component at several depths. We note that the kernels correspond to direct waveform cross-correlation, not the generalized seismological data functionals (GSDF) in Zhao *et al.* (2005). Since the traveltime delay is the volume integration of the product of the kernels and the velocity perturbation (e.g. Dahlen *et al*. 2000), a low-velocity anomaly (negative velocity perturbation) in the negative kernel (red) region, for example, leads to a traveltime delay. Similarly, a low-velocity anomaly in the positive kernel (blue) region results in an earlier arrival. The asymmetry due to the difference in the distances from the interface to the source and receiver is now more obvious. At each depth below the source, the intensity of the kernels (the absolute magnitude) is larger on the source side. Right beneath the layer interface and along the ray path, the sensitivity kernels have weak negative values. The kernels become stronger (larger absolute values) horizontally away from the ray path before changing to positive values (Fig. 6a). The full width of the negative kernels surrounding the ray path is ∼25 km. A local minimum is clearly visible at the piercing point on the receiver side. All these features are consistent with the results of direct waveform simulation and cross-correlation (Figs 3a, 4a and 5).

On the vertical profile half way between the source and receiver and perpendicular to the ray path (Fig. 6b), the sensitivity increases with depth from the interface to a small positive value below the ray path. The small positive area is surrounded by strong negative sensitivities in an approximately half circle. The negative-sensitivity

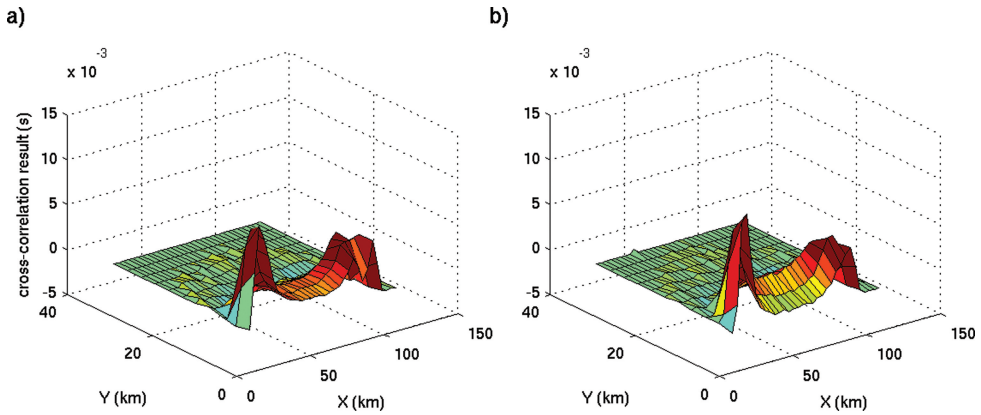


Figure 3. (a) The head wave traveltime delays measured by the cross-correlation of the reference waveform and that with the moving velocity perturbation right beneath the layer interface. (b) The head wave traveltime delay measurements for the same-sized velocity anomaly whose top is 1.6 km below the layer interface. The *x*-axis is the horizontal distance in the direction of the source and receiver path measured from the side of the model; the *y*-axis is the horizontal distance to the source–receiver plane. The two peaks of the traveltime sensitivity are located near the two piercing points of the head wave ray path entering into and leaving the bottom layer. The locations of the two piercing points are ($X = 14.4$ km, $Y = 0$ km; $X = 89.5$ km, $Y = 0$ km). Note that the first zone of relatively high positive values (traveltime delays) is surrounded by a zone of small negative values (earlier arrivals), which in turn is surrounded by a third zone with small positive values.

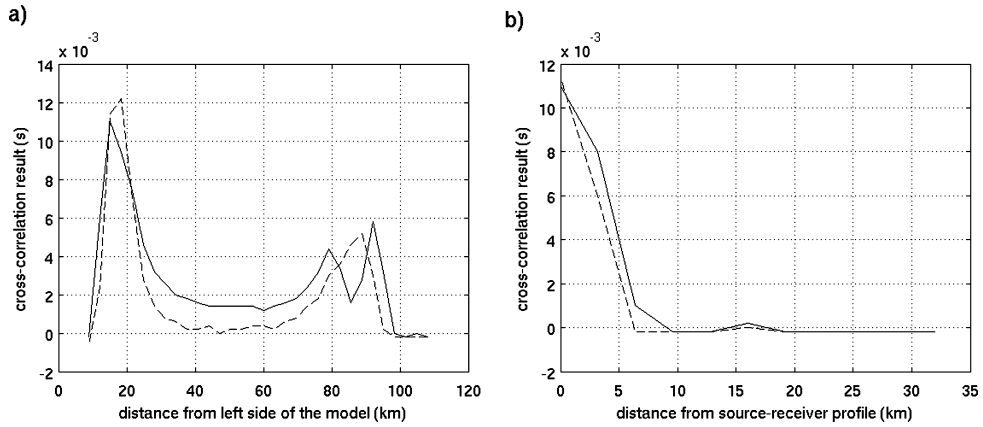


Figure 4. (a) A profile of the traveltime delays (sensitivities) measured by cross-correlating waveforms for models with and without the velocity perturbation along the source–receiver path. The solid line is for the model with the velocity perturbation right beneath the interface (a profile from Fig. 3a) and the dashed line corresponds to the case in which the top of the same-sized perturbation is 1.6 km below the interface (a profile from Fig. 3b). (b) The traveltime sensitivity along a profile perpendicular to the source–receiver path and through the maximum peak near the source ($x = 15.2$ km in Fig. 3). The sizes of the sensitivity region are about the same.

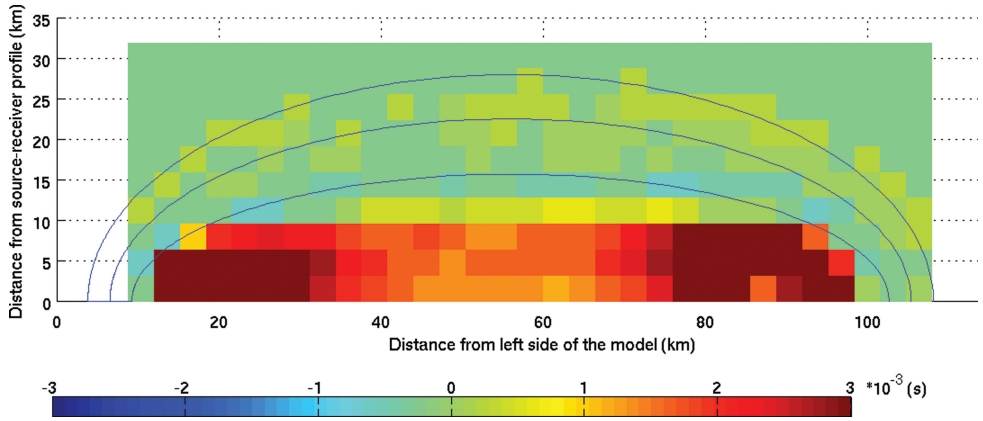


Figure 5. Plan view of Fig. 3(a). Superimposed on the traveltime delays for the velocity perturbation right beneath the interface, the blue lines delineate the boundaries of the first (innermost), second, and third Fresnel zone for the head wave at the interface. The pattern of the areas with positive and negative delays matches approximately with the Fresnel zones.

half ring is in turn surrounded by bands of positive and negative kernels in approximately half circles, which become narrower and weaker away from the ray path.

On the vertical profile containing the source and receiver (Fig. 6c), the kernels resemble those of tuning waves in the upper layer but differ significantly in the lower layer. Again the kernels are weak but non-zero along the ray path below the interface. The sensitivity of the kernels increases with depth from the interface to a small positive value before reaching strong negative sensitivities in the lower layer, the depth of which increases with the distance to the piercing points on the source or receiver side, whichever is smaller. Because the layers are homogeneous, the downward bending of the sensitivity kernels has nothing to do with a vertical velocity gradient in the lower layer and can be understood as the broadening of the Fresnel zones. Unlike the 'banana–doughnut' sensitivity kernels for turning waves, the traveltime kernels for the head wave are located on only one side of the ray path below the interface and thus may be characterized as the 'split banana–doughnut' sensitivity kernels.

The amplitude sensitivity kernels of the head wave for the same model provide us a different perspective of the head wave behaviours (Fig. 7). Comparing the traveltime and amplitude kernels (Figs 6c and 7), we note the strong amplitude sensitivity at the location where the traveltime sensitivity is relatively small below the interface. We also note that the traveltime and amplitude kernels change their polarities (positive or negative values) at different depths. Thus the traveltime and amplitude of head waves provide independent and complementary constraints on the velocity structure. Applications of amplitude kernels to real problems have to account for intrinsic attenuation, which is not addressed in this paper. For this reason, more emphasis is given to the traveltime kernels in the discussion.

To validate the kernel results more quantitatively, we put a cylindrical-shaped anomaly at various depths in the model and measure the traveltime and amplitude anomalies by waveform cross-correlation. The cylindrical-shaped velocity perturbation has a height of 6 km, a radius of 3 km, and the maximum magnitude of +0.03 per cent. The velocity perturbation decreases from the maximum value at the centre of the perturbation to zero on its surface following a square of cosine function. It is at a horizontal location of $X = 61.2$ km, $Y = 64.4$ km (see Fig. 6 for the definition of the coordinates). The kernel predictions match the traveltime and amplitude anomalies from direct waveform cross-correlation very well (Fig. 8), confirming the accuracy of the kernel calculations.

© 2007 The Authors, *GJI*, **171,** 847–856
Journal compilation © 2007 RAS

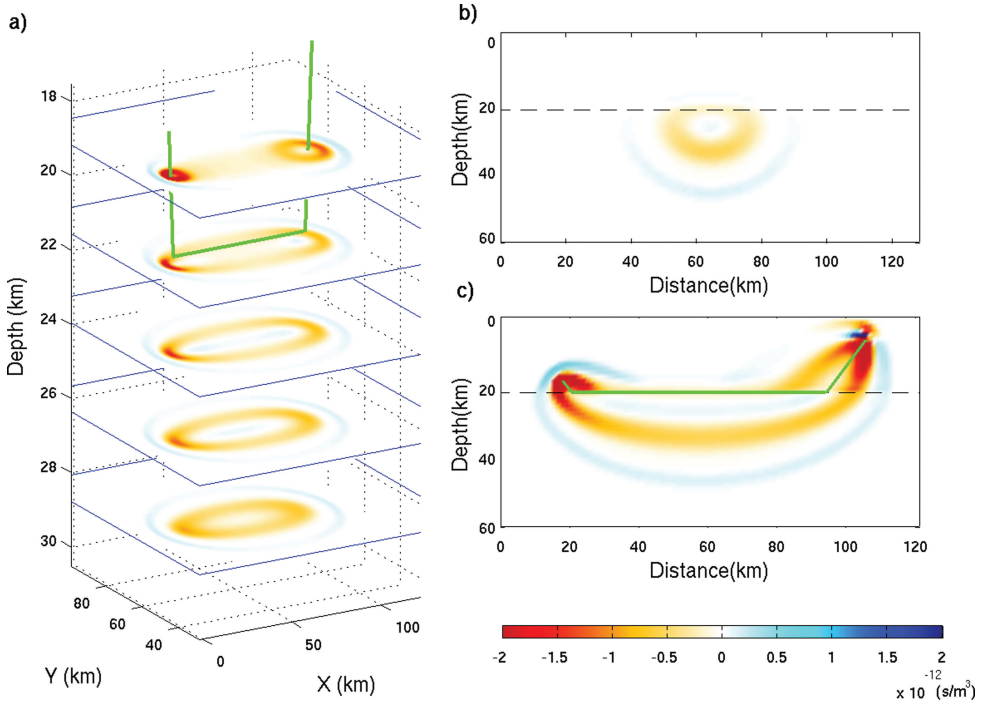


Figure 6. (a) The traveltime sensitivity kernels for the head wave recorded on the vertical component on the horizontal planes at depths below (21.6, 24, 26.4 and 28.8 km) and above (19.2 km) the interface that separates the low and high velocity layers. The green line marks the head wave ray path. The source is located on the left side of this figure. The negative (red colours) and positive (blue colours) values are so defined that a low-velocity anomaly located in the region of the negative kernels results in a traveltime delay and the same velocity perturbation in the region of positive kernels leads to an earlier head wave arrival. Fresnel zones can also be identified as in Fig. 5. (b) The traveltime sensitivity kernel for the head wave on a vertical profile half way between the source and receiver and perpendicular to the ray path. The dashed line is the layer interface. (c) The traveltime sensitivity kernels for the head wave on the vertical profile containing the source and receiver. The full range of the kernels is –1.63 to 1.22 $\times$ 10^{-11} s m^{-3}.

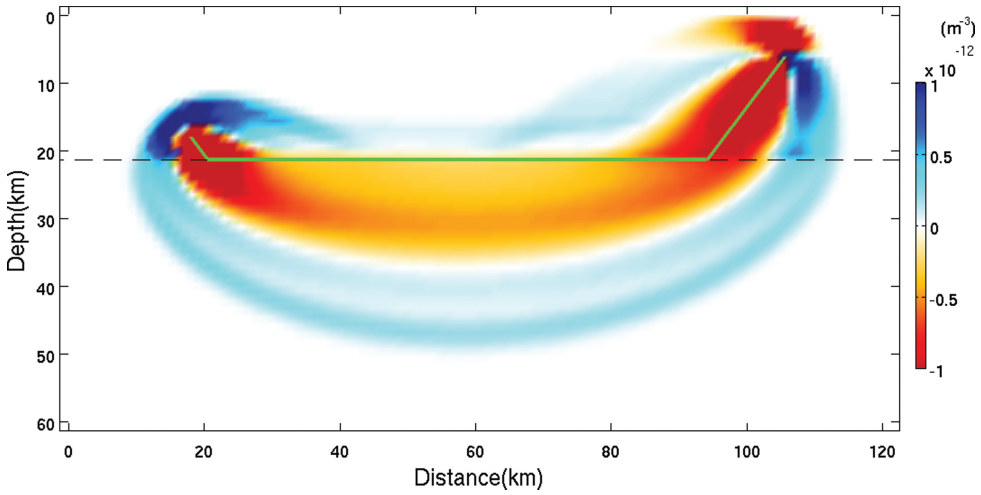


Figure 7. Amplitude sensitivity kernels for the vertical component of the head wave on the vertical profile containing the source and receiver. The dashed line indicates the layer interface and the green line highlights the ray path. The negative (red colours) and positive (blue colours) values are so defined that a low-velocity anomaly in the red region causes an amplitude increase (see Fig. 2 for an example) and the same velocity anomaly in the blue region leads to a reduction in the amplitude of the head wave. The full range of the kernels on this profile is –2.31 to 0.34 $\times$ 10^{-11} m^{-3}.

DISCUSSIONS

Layer interfaces in the real Earth are rarely exact flat, and the regions that are of geological interest usually have complex layer interfaces as well as vertical velocity variations. In this section we expand the study of the finite-frequency Pn wave from the uniform planar layers to more complex structural settings.

Effects of interface topography

Scattering of regional Pn by Moho topography has been observed previously (Kvaerna & Doornbos 1991), but a systematic and quantitative way to determine the effects of Moho topography on the Pn traveltime is still needed. In order to explore the head wave behaviours in media with an irregular interface, we build two

© 2007 The Authors, *GJI*, **171,** 847–856
Journal compilation © 2007 RAS

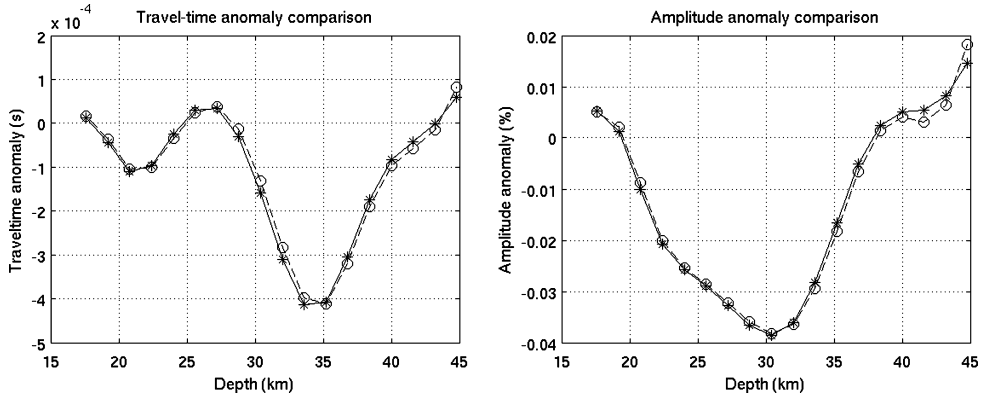


Figure 8. Comparison between the kernel predictions (stars) and the measurements directly from waveform cross-correlation (circles). The horizontal axis is the depth of the centre of the velocity perturbation. See text for the description of the velocity perturbation.

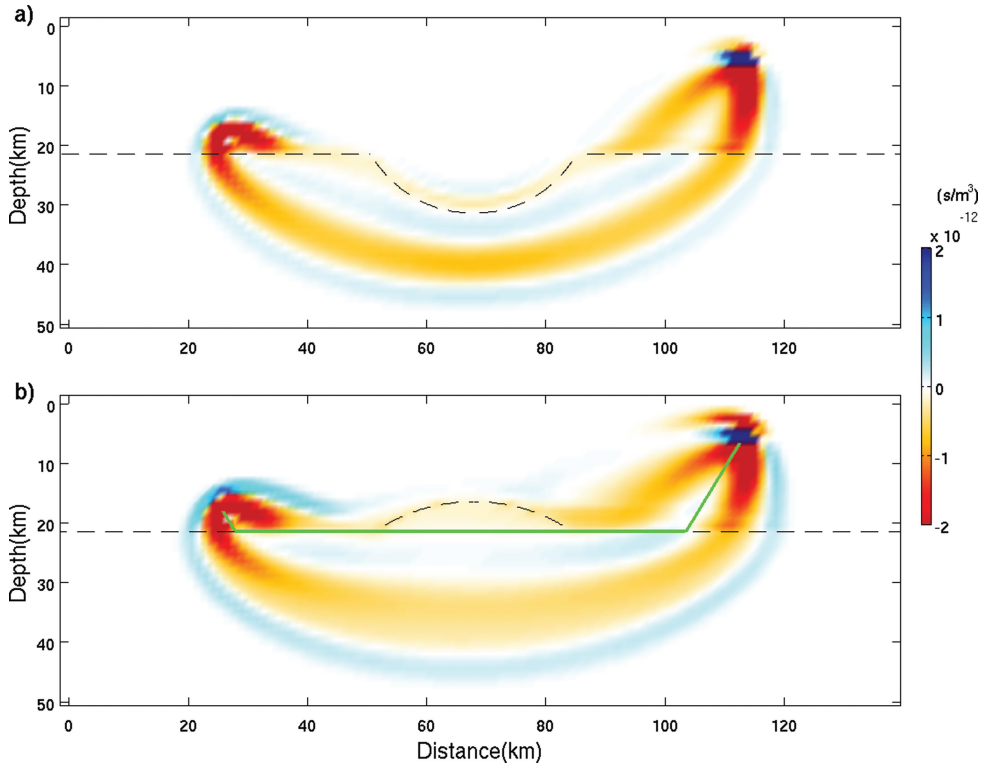


Figure 9. The kernels for the vertical component of head waves in the models with up- and down-bending layer interface between the source and receiver. Except for the perturbed interface, all other parameters of the models are the same as those of the model in Fig. 6. Note that the interface variation is cylindric with the symmetric axis perpendicular to the plane containing the source–receiver path, not spherical. The dashed line indicates the layer interface and the green line highlights the head wave ray path. The meanings of the positive and negative values are the same as those in Fig. 6. (a) A cylindrical down-bending interface with the maximum depression of 10 km and a horizontal dimension of 35 km. The full range of the kernel is –2.37 to 7.05 $\times$ 10^{-11} s m^{-3} (b) An up-bending interface. The maximum shoaling is 5 km, and the horizontal dimension of the interface perturbation is 35 km. The full range of the kernel is –2.48 to 7.37 $\times$ 10^{-11} s m^{-3}.

more models with down-bending and up-bending layer interfaces. Fig. 9(a) shows the traveltime kernel of the vertical component of the head wave for a down-bending interface model. We note that the maximum sensitivity regions beneath the interface are compressed into a smaller horizontal and depth range below the maximum depression of the layer interface. This results in a stronger sensitivity beneath the depression of the interface compared to that in the model with a flat interface. Fig. 9(b) shows the traveltime kernel of the vertical component of the head wave for the model with an up-bending layer interface. In this model, the strong negative sensitivity zones are stretched into a broader horizontal region, resulting in a reduced magnitude of the sensitivity kernels compared to those of the reference model (Fig. 9b).

Effects of vertical velocity gradients

In the real Earth, the upper mantle usually has a positive or negative vertical velocity gradient, instead of being homogeneous. We define a positive velocity gradient as an increase in velocity with depth. In order to understand the effects of the vertical velocity gradient

© 2007 The Authors, *GJI*, **171,** 847–856
Journal compilation © 2007 RAS

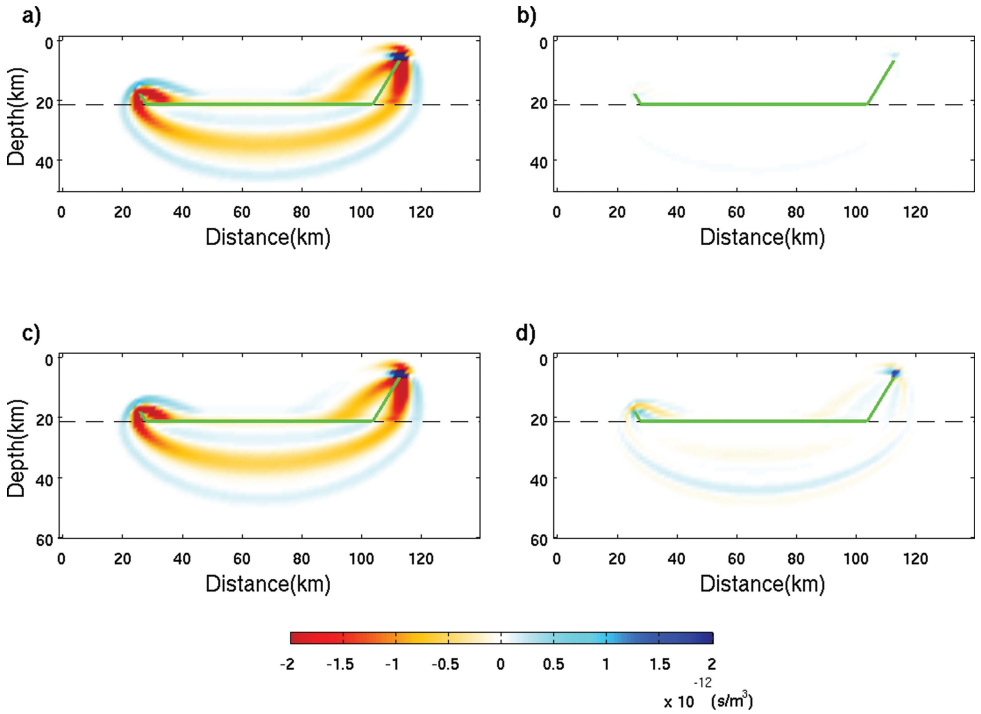


Figure 10. The traveltime kernels for the vertical component of the Pn waves in the model with a vertical gradient of +0.004 km s^{-1} km^{-1} (a) and +0.02 km s^{-1} km^{-1} (c) in the lower layer. The dashed line indicates the layer interface and the green line highlights the ray path. (b) and (d) The differential kernels between the models with and without the two vertical velocity gradients (Figs 6c–10a) and (Figs 6c–10c), respectively. The meanings of the positive and negative values are the same as in Fig. 6.

on the Pn sensitivity kernels, we change the high-velocity layer by introducing a velocity gradient of 0.004 km s^{-1} km^{-1} and keep all other parameters in the model the same. For reference, the earth-sphericity correction on homogeneous layers introduces a positive gradient of about 0.0013 km s^{-1} km^{-1}. The traveltime kernels vary with the vertical velocity gradient, but they are surprisingly very close to those of the reference model with the homogeneous lower layer (Figs 10a and b). A larger velocity gradient of 0.02 km s^{-1} km^{-1}, which is observed in certain areas (Lizarralde *et al*. 2004), causes a larger difference in the traveltime kernels (Figs 10c and d). However, the difference is still about an order of magnitude less than the reference kernel itself (Fig. 6). A model with a negative vertical gradient of –0.004 km s^{-1} km^{-1} in the lower layer also yields the sensitivity kernels that are very close to those of the reference model. A full discussion of the possible nature of the Pn wave in the high-velocity layer with a negative vertical velocity gradient (e.g. Cerveny & Ravindra 1971; Tittgemeyer *et al*. 2000) is beyond the scope of this paper and needs to be further investigated. These results suggest that the Fréchet kernels of the finite-frequency Pn waves are relatively insensitive to the uncertainties in the vertical velocity gradient within a relatively short propagation distance as in the models, and the differences between the finite-frequency kernels and ray predictions are far more pronounced. As the distance between the source and receiver increases, the effect of the velocity gradient is expected to become larger. Depending on the vertical velocity gradient and wave period, a Pn wave may evolve into a

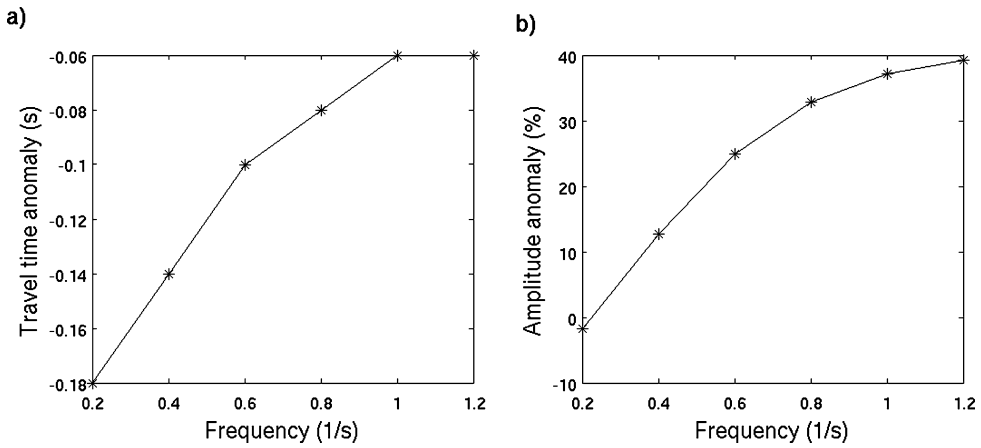


Figure 11. The traveltime (a) and amplitude (b) anomalies of the head wave in the model having a lower layer with a 0.02 km s^{-1} km^{-1} positive velocity gradient relative to those in the model with the homogeneous lower layer at different frequencies.

separable mantle turning wave and interference waves at greater distances (Cerveny & Ravindra 1971; Nowack & Stacy 2002); in such a case, the sensitivity kernels of the first Pn arrival become more like those of regular mantle turning waves (e.g. Dahlen *et al*. 2000), but still differ from those of ray theoretical predictions. On the other hand, if we include a long enough Pn coda, the whispering gallery waves could affect the kernels.

Dispersion of Pn waves

We have shown that the pattern of the Fréchet kernels roughly matches with the predicted Fresnel zones (Fig. 5) and thus the depth range of the traveltime sensitivity below the interface increases with the wavelength and propagation distance. Like Rayleigh waves, finite-frequency Pn and Sn waves are expected to be dispersive if the velocity structure in the lower layer has a gradient with depth. To verify this, we compare the Pn wave travelled through the model having a lower layer with a positive gradient of 0.02 km s^{-1} km^{-1} with that calculated from the reference model with a uniform lower layer. The traveltime and amplitude anomalies of the Pn waves at different frequencies are measured with the GSDF method (Gee & Jordan 1992). The head wave is dispersive in the model with a lower layer having a positive gradient. The longer period waves arrive earlier than the shorter period waves (Fig. 11). This can be attributed to the fact that the longer-period waves have a deeper sensitivity below the interface where the velocity is higher. As expected, the amplitude of the Pn wave in the model with a positive velocity gradient in the lower layer is overall larger than that of a uniform lower layer. Together with the deepening of the maximum sensitivity region with the propagation distance due to the broadening of the Fresnel zones, the frequency dependence of the Pn traveltime and amplitude may provide important constraints on the vertical velocity gradient in the mantle lithosphere.

CONCLUSIONS

The sensitivity of the finite-frequency head wave is very different from that predicted by ray theory. While in ray theory traveltime and amplitude anomaly is sensitive only to velocity perturbation along the geometric ray path and the sensitivity is the same along the ray path, our results show that realistic head waves with finite frequencies are sensitive to the 3-D structure in a complex way. Below the interface, the peak traveltime and amplitude sensitivity is located near the two piercing points of the geometric ray entering and leaving the interface. The sensitivity is much smaller at other points on the geometric ray path. The pattern of positive and negative sensitivities approximately matches with the Fresnel zones, with the traveltime and amplitude anomaly most sensitive to velocity perturbations in the first Fresnel zone. Unlike the turning waves, the sensitivity right beneath the interface is non-zero along the source–receiver path. The sensitivity beneath the layer interface is strong at some distance from the ray path, depending on the wavelength and propagation distance. There is a small positive region in the traveltime sensitivity kernel surrounded by relatively strong negative sensitivity kernels below the interface. The interface topography has significant effects on the sensitivity kernels. The depression or shoaling of the interface compresses or stretches, respectively, the traveltime sensitivity kernels, resulting in increased or decreased sensitivities beneath the interface topography. Because the distribution of the Fréchet kernels is a function of wavelength, head waves are dispersive if the velocity structure in the lower layer has a gradient with depth. Thus the finite-frequency head wave kernels, which account for the possible frequency dependence of the Pn and Sn traveltime and amplitude, may provide a powerful tool to constrain the vertical velocity gradient in the mantle lithosphere and extend the Pn and Sn tomography from presently 2-D to 3-D.

ACKNOWLEDGMENT

The finite-difference waveform simulation code is provided by Kim B. Olsen. Comments from two anonymous reviewers helped improve the manuscript. This work was supported by Air Force Research Laboratory FA8718–06-C-0014 and U.S. National Science Foundation under grant no. 0241655.

REFERENCES

Aki, K. & Richards, P.G., 2002. *Quantitative Seismology*, University Science Books, Sausalito, California.

Bannister, S.C., Ruud, B.O. & Husebye, E.S., 1991. Tomographic estimates of the sub-Moho seismic velocities in fennoscandia and structural implications, *Tectonophysics*, **189,** 37–53.

Båth, M., 1966. Propagation of Sn and Pn to teleseismic distances, *Pure Appl. Geophys.*, **64,** 19–30.

Berry, M.J. & West, G.G., 1966. Reflected and head wave amplitudes in a medium of several layers, in *The Earth Beneath Continents*, Geophysical Monograph 10. Washington, DC., American Geophysical Union.

Brazier, R.A., Nyblade, A.A., Langston, C.A. & Owens, T.J., 2000. Pn wave velocities beneath the Tanzania craton and adjacent rifted mobile belts, East Africa, *Geophys. Res. Lett.*, **27,** 2365–2368.

Cerveny, V. & Ravindra, R., 1971. *Theory of Seismic Head Waves*, University of Toronto Press, Toronto.

Dahlen, F.A., Hung, S.-H. & Nolet, G., 2000. Fréchet kernels for finite frequency traveltimes-I. Theory, *Geophys. J. Int.*, **141,** 157–174.

Gee, L.S. & Jordan, T.H., 1992. Generalized seismological data functionals, *Geophys. J. Int.*, **111,** 363–390.

Hearn, T.M., Wang, S., Ni, J.F., Xu, Z., Yu, Y. & Zhang, X., 2004. Uppermost mantle velocities beneath China and surrounding regions, *J. geophys. Res.*, **109,** doi:10.1029/2003JB002874

Hung, S.-H., Dahlen, F.A. & Nolet, G., 2000. Fréchet kernels for finite frequency traveltimes-II. Examples, *Geophys. J. Int.*, **141,** 175–203.

Kvaerna, T. & Doornbos, D.J., 1991. Scattering of regional Pn by Moho topography, *Geophys. Res. Lett.*, **18,** 1273–1276.

Langston, C.A., 1982. Aspects of Pn and Pg propagation at regional distances, *Bull. Seismol. Soc Am.*, **72,** 457–471.

Lay, T. & Wallace, T.C., 1995. *Modern Global Seismology*, **vol. 58**, *Inter. Geophys. Ser.*, Academic Press, San Diego, Calif.

Liu, Q. & Tromp, J., 2006. Finite frequency sensitivity kernels based on adjoint method, *Bull. Seismol. Soc Am.*, **96,** 2383–2397.

Lizarralde, D., Gaherty, J.B., Collins, J.A., Hirth, G. & Kim, S.D., 2004. Spreading-rate dependence of melt extraction at mid-ocean ridges from mantle seismic refraction data, *Nature*, **432,** 744–747.

Marcinkovich, C. & Olsen, K.B., 2003. On the implementation of perfectly matched layers in the fourth-order velocity-stress finite-difference scheme, *J. geophys. Res.*, doi:10.1029/2002JB002235.

Menke, W. & Richards, P.G., 1980. Crust-mantle whispering gallery phases: a deterministic model of teleseismic Pn wave propagation, *J. geophys. Res.*, **85,** 5416–5422.

Menke, W. & Richards, P.G., 1983. The horizontal propagation of P waves through scattering media: analog model studies relevant to long-range Pn Propagation, *Bull. Seismol. Soc Am.*, **73,** 125–142.

Morozov, I.B., Morozova, E.A., Smithson, S.B. & Solodilov, L.N., 1998. On the nature of the teleseismic Pn phase observed on the ultralong-range profile "Quartz" Russia, *Bull. Seismol. Soc. Am.*, **88,** 62–73.

Nolet, G., Coutlee, C. & Clouser, R., 1998. Sn velocities in western and eastern North America, *Geophys. Res. Lett.*, **25,** 1557–1560.

© 2007 The Authors, *GJI*, **171,** 847–856
Journal compilation © 2007 RAS

Nowack, R.L. & Stacy, S.M., 2002. Synthetic seismograms and wide-angle seismic attributes from the Gaussian beam and reflectivity methods for models with interfaces and velocity gradients, *Pure Appl. Geophys.*, **159,** 1447–1464.

Olsen, K.B., 1994. Simulation of three-dimensional wave propagation in the Salt Lake Basin, PhD thesis. University of Utah, Salt Lake City, Utah, 157p.

Ritzwoller, M.H., Barmin, M.P., Villasenor, A., Levshin, A.L. & Engdahl, E.R., 2002. Pn and Sn tomography across Eurasia to improve regional seismic event locations, *Tectonophysics*, **358,** 39–55.

Ryberg, T., Tittgemeyer, M. & Wenzel, F., 2000. Finite difference modelling of P-wave scattering in the upper mantle, *Geophys. J. Int.*, **141,** 787–800.

Tittgemeyer, M., Wenzel, F. & Fuchs, K., 2000. On the nature of Pn, *J. geophys. Res.*, **105,** 16 173–16 180.

Tromp, J., Tape, C. & Liu, Q., 2005. Seismic tomography, adjoint methods, time reversal and banana–doughnut kernels, *Geophys. J. Int.*, **160,** 195–216.

Zhao, L. & Jordan, T.H., 2006. Structural sensitivities of finite-frequency seismic waves: a full-wave approach, *Geophys. J. Int.*, **165,** 981–990.

Zhao, L.S. & Xie, J., 1993. Lateral variation in compressional velocities beneath the Tibetan Plateau from Pn travel time tomography, *Geophys. J. Int.*, **115,** 1070–1084

Zhao, L., Jordan, T.H. & Chapman, C.H., 2000. Three-dimensional Fréchet differential kernels for seismic delay times, *Geophys. J. Int.*, **141,** 558–576.

Zhao, L., Jordan, T.H., Olsen, K.B. & Chen, P., 2005. Fréchet kernels for imaging regional earth structure based on three-dimensional reference models, *Bull. Seismol. Soc. Am.*, **95,** 2066–2080.

© 2007 The Authors, *GJI*, **171,** 847–856
Journal compilation © 2007 RAS